

Stellar haloes in Milky-Way mass galaxies: From the inner to the outer haloes

Patricia B. Tissera^{1,2}, Timothy C. Beers^{3,4}, Daniela Carollo⁵, Cecilia Scannapieco⁶

¹ *Consejo Nacional de Investigaciones Científicas y Técnicas, CONICET, Argentina.*

² *Instituto de Astronomía y Física del Espacio, Casilla de Correos 67, Suc. 28, 1428, Buenos Aires, Argentina.*

³ *National Optical Astronomy Observatory, Tucson, AZ, 85719 USA.*

⁴ *JINA: Joint Institute for Nuclear Astrophysics.*

⁵ *Department of Physics and Astronomy, Macquarie University, Sydney, 2109 NSW, Australia.*

⁶ *Leibniz-Institut für Astrophysik Potsdam (AIP), An der Sternwarte 16, D-14482 Potsdam, Germany.*

21 August 2018

ABSTRACT

We present a comprehensive study of the chemical properties of the stellar haloes of Milky-Way mass galaxies, analysing the transition between the inner to the outer haloes. We find the transition radius between the relative dominance of the inner-halo and outer-halo stellar populations to be $\sim 15 - 20$ kpc for most of our haloes, similar to that inferred for the Milky Way from recent observations. While the number density of stars in the simulated inner-halo populations decreases rapidly with distance, the outer-halo populations contribute about 20 – 40 per cent in the fiducial solar neighborhood, in particular at the lowest metallicities. We have determined $[\text{Fe}/\text{H}]$ profiles for our simulated haloes; they exhibit flat or mild gradients, in the range $[-0.002, -0.01]$ dex kpc^{-1} . The metallicity distribution functions exhibit different features, reflecting the different assembly history of the individual stellar haloes. We find that stellar haloes formed with larger contributions from massive subgalactic systems have steeper metallicity gradients. Very metal-poor stars are mainly contributed to the halo systems by lower-mass satellites. There is a clear trend among the predicted metallicity distribution functions that a higher fraction of low-metallicity stars are found with increasing radius. These properties are consistent with the range of behaviours observed for stellar haloes of nearby galaxies.

Key words: Galaxy: structure, galaxies:formation, galaxies:evolution, cosmology: theory

1 INTRODUCTION

The formation of diffuse, extended stellar haloes is a natural result of hierarchical clustering scenarios, where most of the stars are acquired by the accretion of satellites that are completely or partially disrupted (e.g. Bullock & Johnston 2005; Johnston et al. 2008; Cooper et al. 2010; Font et al. 2011; Tissera et al. 2012). Numerical simulations have also indicated the existence of an in situ stellar halo component formed dissipatively in the inner regions and/or by disheated stars (e.g. Zolotov et al. 2009; McCarthy et al. 2012). The contributions of each type of stellar populations reflect the histories of assembly of the stellar haloes, as well as the physics included in the simulations. Disentangling their individual effects is a challenging task. In this paper, we study a suite of six Milky-Way mass galaxies, resolved with intermediate numerical resolution, with the aim of constructing a

more complete picture of the assembly of galaxies and their stellar haloes.

Most of the baryonic physics in current galaxy formation models are described through the use of subgrid physics; these models have improved significantly in the last few decades. As a consequence, it is now possible to describe, on a more physical basis, the formation of galaxy discs, mass-loaded gas outflows and the chemical evolution of gas and stars (e.g. Agertz et al. 2009; Governato et al. 2009; Scannapieco et al. 2009; Guedes et al. 2011). Other trends, such as the dependence of star-formation efficiency on total mass, remain to be fully explained (e.g. Aumer et al. 2013; De Rossi et al. 2013). Nevertheless, all such models carry with them theoretical or numerical caveats that can be constrained through confrontation with observations.

It is now well-established that the observed chemodynamical patterns of galaxies provide powerful tools for

the interpretation of observations and for efforts to improve galaxy formation models. In particular, regarding the Milky Way (MW), the plethora of such information that will flow in the near future from the Gaia satellite, as well as from other large-scale ground-based efforts (for a recent review, see Ivezić et al. 2012) will dramatically expand the scope of the observational constraints. There is already evidence for the existence of two stellar halo populations in the MW, with different properties (e.g. Carollo et al. 2007, 2010; Beers et al. 2012; An et al. 2013). Recent reports on nearby galaxies, such as M31 and M81, also show evidence for the existence of stellar haloes with complex structure (Gilbert et al. 2013; Ibata et al. 2014; Monachesi et al. 2013). Observations are also starting to provide information on the stellar haloes at high redshift, opening the possibility of constraining the assembly of the stellar haloes directly (Trujillo & Bakos 2013).

The properties of the baryons and the dark matter in the re-simulated version of the Aquarius haloes by Scannapieco et al. (2009) have been analysed in a series of papers. From these works, we know that none of these haloes hosts a disk-like galaxy resembling the MW, but instead, galaxies with a variety of morphology have been formed. Scannapieco et al. (2009) and Scannapieco et al. (2011) find that the discs are generally young, with stars spanning a wide range in stellar age. The younger stars are on circular orbits, defining thin discs, while the oldest stars determine thicker discs with 2-3 times larger velocity dispersion than the thin components. Most of the stars in the discs formed from gas accreted onto the main progenitor to first build up gaseous discs. The bulge components formed early, and in shorter starbursts. The stellar haloes are reported to have a complex structure, with most of their mass coming from accreted satellites. The chemical patterns of these dynamical components have been extensively discussed by Tissera et al. (2012, hereafter, Paper I) and Tissera et al. (2013, hereafter, Paper II). In Paper I we analysed the chemical properties of the discs, bulge, and inner- and outer-halo populations in relation to their assembly histories, finding that the [Fe/H] and the α -elements trends are in very good agreement with observations. In particular, in Paper II, we highlighted how one might understand a range of the properties observed in the stellar haloes of MW-mass galaxies (e.g., metallicity distribution functions, MDFs, α -element enrichment histories, density distributions, and kinematics) in the context of their Λ CDM hierarchical halo assembly histories. In our previous works, we analysed the inner- and outer-halo populations as separate components.

In this paper, we continue our analysis of the nature of the predicted stellar populations of a suite of MW-mass galaxies, selected from the Aquarius simulation project, but focus on the stellar haloes as a whole, and their dependence on the accretion history of satellites. We aim at studying in more detail the superposition of the inner-halo populations and outer-halo populations, how they vary from one simulated system to another, and how the transition from the inner-halo regions to the outer-halo regions can be linked to their assembly histories. We concentrate on the analysis of the accreted satellites, since they are the main contributors to the formation of the stellar haloes in our adopted cosmological model, and how the history of their assembly could be linked to the characteristics of the MDF as a function

of radius. We discuss implications for the interpretation of observational data in the MW and other large spirals, and on the development of predictions that might be used to test and refine future simulations.

In Section 2 we describe the simulations and the main aspects of our chemical-evolution model. In Section 3 we consider the transition between the inner-halo populations and the outer-halo populations, as well as the predicted combined MDFs and the expected abundance profiles. In Section 4 we analyse the nature of the satellites that contributed to the formation of the stellar haloes, and compare how they differ with respect to the contribution of stars with different metallicities to the formation of the stellar haloes. In Section 5 we study very metal-poor stars in particular, and compare their frequency as a function of distance with available observations. We summarize our findings in Section 6, and provide a brief discussion.

2 THE SIMULATED STELLAR HALOES

We continue our analysis of the suite of six high-resolution MW-mass systems described in Papers I and II. These six haloes are part of the Aquarius simulation project presented by Scannapieco et al. (2009). The Aquarius haloes were selected from a cosmological volume of a 100 Mpc h^{-1} box, with only a mild isolation criterion imposed at $z=0$ (see Springel et al. 2008, for further details on the generation of the initial conditions). The initial conditions used in this paper have been modified to include baryons (Scannapieco et al. 2009).

The simulations were performed with a Λ CDM cosmogony with $\Omega_m = 0.25$, $\Omega_\Lambda = 0.75$, $\sigma_8 = 0.9$, $n_s = 1$, and $H_0 = 100 h \text{ kms}^{-1}\text{Mpc}^{-1}$ with $h = 0.73$. The galactic systems are identified at the virial radius (r_{200}), and have virial masses in the range $\approx 5 - 11 \times 10^{11} M_\odot h^{-1}$. They are numerically resolved using ≈ 1 million total particles within the virial radius, so that dark matter particles have masses of the order $\approx 10^6 M_\odot h^{-1}$, while initially the gas particles have masses of $\approx 2 \times 10^5 M_\odot h^{-1}$. Table 1 summarizes their principal characteristics.

The simulations were run using a modified version of GADGET-3 (Scannapieco et al. 2005, 2006), which explicitly describes the physics of the baryons, including their chemical evolution from the contributions of Type II and Type Ia supernovae (hereafter, SN). The SN feedback allows for the triggering of galactic mass-loaded outflows, self-regulated by the potential well of the systems. A detailed description of the chemical model and SN-feedback mechanisms can be found in Scannapieco et al. (2009). This SN-feedback scheme has proven successful for the regulation of the star-formation activity during violent and quiescent stages of evolution. One of its most important features is the non-existence of mass-size dependent parameters, which makes this implementation well-suited to study of the formation of galaxies in a cosmological context. However, in the current set of Aquarius-simulated haloes, there is still an overproduction of stars at high redshift. This is a complex, open problem for current galaxy formation models, and an area of active research (e.g. Aumer et al. 2013; Hopkins et al. 2013; Stinson et al. 2013). Nevertheless, these haloes allow us to study and compare their properties in relation to their his-

tory of assembly, given that all of them have been run with the same numerical model.

In Papers I and II, the effects of numerical resolution on the physical properties of the structure have been extensively discussed. In Paper I we analysed three different levels of resolution, in order to assess numerical effects on the derived chemical properties. We found that, for the global analysis we performed, the current resolution was sufficient. We estimated the mass fraction of stars with $[\text{Fe}/\text{H}] < -2.5$ within the virial radius, for the three level of resolution, finding that the percentages converge from the very low resolution ($\sim 7\%$ in Aq-E-7) to the highest available ($\sim 5\%$ in Aq-E-6 and Aq-E-5). However, some properties of the simulated haloes might be more sensitive to numerical effects; below we alert the reader where those might be a concern.

2.1 The Aquarius stellar haloes

In Paper I, three main dynamical components were defined: the discs, central spheroids, and stellar haloes, by adopting simple binding-energy criteria. Briefly, this method uses the ratio between the angular momentum along the major axis of rotation and the total angular momentum of the systems, ϵ , to define the disc component ($\epsilon > 0.65$). The remaining particles are assigned membership in the central spheroids, the inner-halo populations (hereafter, IHPs) and the outer-halo populations (hereafter, OHPs) by application of a binding-energy criterion, as described in detail in Papers I and II. Simple energy criteria were used to define these haloes, with the higher-energy (less-bound) stars belonging to the OHPs, and the lower-energy (more-bound) stars belonging to the IHPs. The surviving satellites are not considered in this analysis. There are, however, certainly debris streams that have not been totally disrupted present in the simulated stellar haloes, as can be seen from see Fig. 1 in Paper I. Their quantification as separate substructures might be limited by numerical resolution (Gómez et al. 2013), but this does not directly impact our results. We are interested in analysing them as part of the OHPs or IHPs to which they are assigned on the basis of their dynamical properties.

The binding-energy criterion we employ does not establish a sharp spatial boundary between the populations of these components; rather, they are superposed on one another. Hence, it is convenient to distinguish, as was done in Paper II, between the inner-halo and outer-halo regions (IHRs and OHRs, respectively), within which the corresponding IHPs and OHPs dominate. We refer to the radial distance where the transition from the IHRs to the OHRs occurs as the halo transition radius, r_{HTR} .

According to the results of our previous work, the OHPs mainly comprise low-metallicity, highly α -element enriched stars (the so-called debris subpopulation) assembled from accreted satellites. The level of enrichment of the OHPs correlates with the fraction of these stars which were formed in more-massive satellites, with dynamical masses larger than $10^9 M_{\odot}$. Some satellites will be able to survive farther into the potential well of their parent galaxies, and although they are disrupted by dynamical friction during their infall, they can contribute to the formation of a weak metallicity gradient in the outer haloes. These systems could be gas-rich, so that star formation might continue within the virial haloes of their parent galaxies (see Sawala et al. 2012, for a detailed

analysis of the evolution of the satellites in Aq-C-5). These stars were called the endo-debris subpopulation, and were found to be low metallicity, but less α -enriched, than the debris stars. In Paper II it was shown that the metallicity gradients in the OHPs increased as the contribution from stars formed in more-massive (more-bounded) satellites increased, as expected. Since no clear difference was found in the kinematics of the stars arising from the debris and the endo-debris stars, they were considered as a single population in the outer haloes.

The inner haloes are more complex, and in our simulations their assembly appears to have involved three different components: debris stars, endo-debris stars and disc-heated stars. Each of the Aquarius haloes exhibit the three subpopulations in different proportions, depending on their formation history. It was shown in Paper II that accreted stars cover the entire range of binding energies of the inner haloes, while the endo-debris and disc-heated stars are more gravitationally bound. Most of the IHP stars have ages larger than ~ 8 Gyr, with an average age around ~ 11 Gyr. The endo-debris and disc-heated stars exhibit lower levels of α -element enrichment. The younger disc-heated stars are supported more by rotational motions, while the older of them exhibit cooler kinematics, similar to those of the accreted stars. The endo-debris stars exhibit slightly larger velocity dispersions.

Overall, our simulated haloes are assembled from stars formed in satellites that were accreted by the main progenitor galaxy, or from the gas retained by incoming satellites that was later transformed into stars and/or tidally disrupted. A mean contribution of ~ 25 per cent of stars in the IHPs comes from disc-heated stars¹. The fraction varies between 3 – 30 per cent as a consequence of their different assembly histories. The disc-heated stars in our simulations are, in general, older than 8 Gyr; only the younger population is able to recall its origin, because of the remaining excess of rotational velocity in comparison with other stellar-halo stars (see fig. 1 of Paper II). And, while having been formed in a disc structure, they were disturbed and dynamically heated by violent events, as found in previous works (e.g. Abadi et al. 2003; Purcell et al. 2009). On average, these stars have lower α -enhancement and lower metallicity than those formed in accreted satellites (Zolotov et al. 2010). Recent observations have reported the existence of stars with dynamical and chemical properties in agreement with their being disc-heated stars in the stellar haloes of the MW (Nissen & Schuster 2010) and M31 (Dorman et al. 2013). The frequency and properties of these stars can be reproduced by our simulations.

Since, in this work, we focus our analysis on the entire stellar haloes of massive spiral galaxies, it is interesting to ask if the surviving satellite systems in the simulated haloes are comparable to the current state-of-knowledge of the orbiting satellites in the MW and M31. Therefore, we estimated the number of satellites as a function of the stellar masses, and compared them with observations from

¹ The fraction of disc-heated stars in our simulations should be considered upper limits, due to numerical limitations. Because of the gravitational softening is $\sim 1 \text{ kpc} h^{-1}$, the discs are already thick.

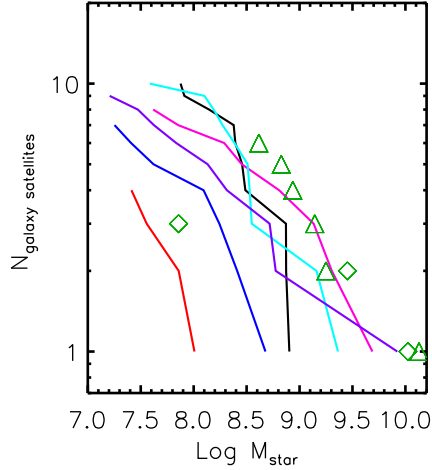


Figure 1. Number of surviving satellites in the simulated Aquarius haloes as a function of their stellar masses (see Table 1 for colour code). The observed distributions for the MW (green diamonds) and M31 (green triangles) taken from McConnachie (2012) and Watkins et al. (2013), respectively, have been included for comparison.

McConnachie (2012) and Watkins et al. (2013). We only consider systems resolved with at least 1000 particles, since otherwise their properties could be strongly affected by the resolution of the simulations. These satellite systems have been also analysed in Paper I, where it was shown that they possess diverse star-formation histories and metallicity distributions. In fact, on average, our surviving satellites tend to be α -element poor with respect to those satellites accreted to form the stellar haloes (which also tend to be α -element poor). As can be seen from Fig. 1, the analysed Aquarius haloes show a variety of satellite distributions, as expected. The observed relations corresponding to MW and M31 are within the simulated values, at least for the mass range analysed in this work.²

3 THE TRANSITION BETWEEN THE IHPs AND OHPs

As shown in Papers I and II, the IHPs and OHPs of the different simulated haloes exhibit different chemical and dynamical properties, reflecting their different assembly histories. In these previous papers, their physical properties were studied individually. However, observers detect the superposed populations “as is,” requiring them to interpret their findings in order to satisfactorily confront them with galaxy formation models. Motivated by this simple reality, we have considered the nature of the superposed IHPs and OHPs together, and attempt to glean information about their observed characteristics in relation to the different halo-assembly histories.

We analyse how the IHPs and OHPs are superposed with one another within the main-galaxy virial radius. Fig. 2

² We assume a mass-to-light ratio of 4.8 to convert observed luminosities in the V-band to stellar masses.

shows the stellar mass fraction of these populations in equal-radial intervals for each simulated halo. This immediately allows for the determination of the spatial limits of the IHR and OHR for each halo, specified here as r_{HTR} . From inspection of this figure, we can clearly see that the IHPs dominate within r_{HTR} , while for larger radii, the OHPs are the main contributors. We find $r_{\text{HTR}} \sim 15 - 20$ kpc for five out of the six analysed haloes, similar to the inferred transition region for the MW by Carollo et al. (2007, 2010) and de Jong et al. (2010). The only exception is Aq-B-5, which exhibits a transition between the IHR and OHR around $r_{\text{HTR}} \sim 36$ kpc, similar to that found for M31 by Gilbert et al. (2013). In the case of the simulation, this is due to the important contribution of accreted stars to the IHP in comparison to the in situ components. This halo is the only one where the accreted stars dominate over the in situ stars in the IHP, as can be seen from fig. 3 in Paper II (note that the in situ stars tend to be more concentrated and have lower binding energies). The contribution of the OHPs within ~ 10 kpc varies between ~ 10 per cent and ~ 40 per cent, while the IHPs can extend farther into the OHRs, with contributions smaller than ~ 20 per cent in our simulated systems. As shown in Papers I and II, the OHPs are mainly formed from debris stars, while the IHPs received significant contributions from in situ (disc-heated and endo-debris stars) as well as from debris stars. Nevertheless, the fraction of debris stars within $5 - 20$ kpc varies from ~ 30 per cent to ~ 60 per cent of the combined stellar haloes (i.e., the IHPs + OHPs considered together). Within the IHRs, the OHPs and IHPs are superposed, and present a challenge for interpretation of the individual subpopulations if a hierarchical clustering scenario applies. The transition between the IHPs and OHPs is expected to produce a transition in the observed MDFs as one progresses from the IHRs to the OHRs.

3.1 The diffuse stellar halo MDF

The previous analysis suggests that the expected MDFs in the diffuse IHRs of MW-mass galaxy haloes are not the same as the MDFs in the diffuse OHRs of the haloes. According to our models, as one moves outwards, the MDF should change in nature (and shape), decreasing in average metallicity as the different populations contribute in different proportion. How these changes are produced, and whether they store information on the assembly history of a given galaxy, are the questions on which we focus in this section.

Fig. 3 shows the predicted MDFs for stars in the entire stellar haloes, estimated in concentric shells of 20 kpc width (left-hand panels). As the distance to each shell increases, the MDFs tend to shift to lower metallicity, although each of simulated stellar haloes behaves differently in detail. Some haloes exhibit large displacements toward lower $[\text{Fe}/\text{H}]$, while others show only small changes. In all cases, the IHRs exhibit the highest level of chemical enrichment. In particular, it is interesting to note that the simulated halo of Aq-C-5 exhibits negligible abundance variations, even though this halo, just like the others, was formed in a hierarchical clustering scenario. Clearly, a wide range of behaviour can be expected from halo system to halo system.

The different behaviours in the simulated MDFs as a function of distance can be understood from inspection of the cumulative mass fractions of stars as a function of

Table 1. General characteristics of the Aquarius stellar haloes. The left columns indicate the encoding name, the colours and symbols of the simulations used in our figures, all simulated with numerical resolution level-5. N_{dm} and N_{bar} are the total number of particles in each mass component per halo. The parameters r_{200} and M_{200} are the virial radius and mass, respectively. M_s is the stellar mass of the main galaxies hosted by the halo measured within the galaxy’s radius. The last two columns show r_{HTR} , the transition radius between the IHPs and OHPs, and $[\text{Fe}/\text{H}]_{\text{slope}}$, the gradient for the metallicity profiles measured from r_{HTR} to r_{200} .

Systems	N_{dm}	N_{bar}	r_{200} kpc h^{-1}	M_{200} $10^{12} M_{\odot} h^{-1}$	M_s $10^{10} M_{\odot} h^{-1}$	r_{HTR} kpc	$[\text{Fe}/\text{H}]_{\text{slope}}$ dex kpc^{-1}
Aq-A-5 (black crosses)	529110	425737	169	1.10	5.92	18	-0.006
Aq-B-5 (red squares)	435330	354976	132	0.52	2.53	36	-0.007
Aq-C-5 (magenta asterisks)	681143	647325	173	1.18	5.93	15	-0.002
Aq-D-5 (cyan open circles)	599438	460845	171	1.09	4.41	19	-0.008
Aq-G-5 (violet crosses)	679177	778397	143	0.68	5.63	16	-0.002
Aq-H-5 (light green filled circles)	515392	569595	133	0.53	4.73	14	-0.007

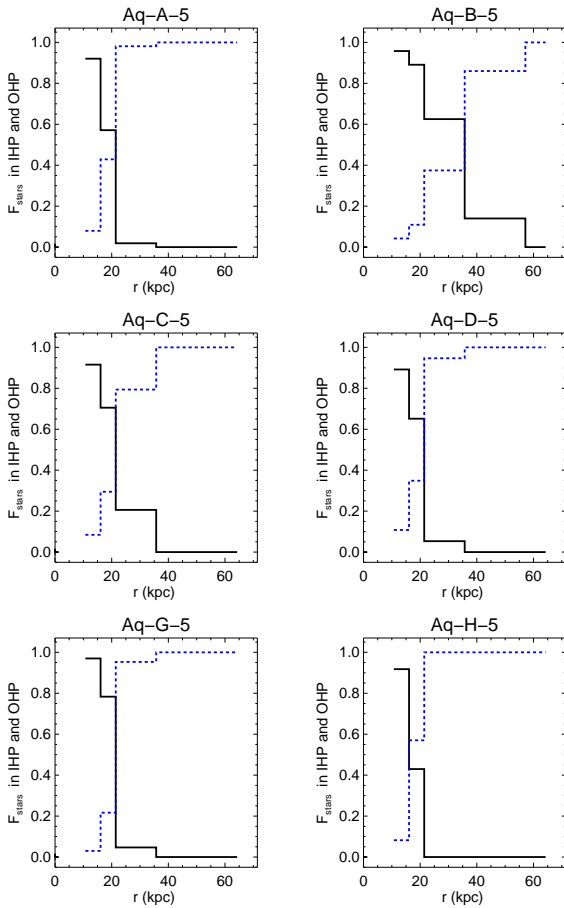


Figure 2. Stellar mass fraction in the IHPs and OHPs, as a function of radius. The radial distance at which the two populations change in relative dominance is taken as the halo transition radius, r_{HTR} . The IHRs are dominated by the IHPs, but there exists a contribution from the OHPs of $\sim 10 - 40$ per cent within r_{HTR} , increasing dramatically for larger radii.

$[\text{Fe}/\text{H}]$, for different distances, shown in the middle panels of Fig. 3. Although the simulated stellar haloes share some features in common, they also exhibit a variety of differences in the MDFs from shell to shell. While some systems exhibit similar fractions of very metal-poor (VMP; $[\text{Fe}/\text{H}] < -2$) stars at all radii (e.g., Aq-C-5), others exhibit a tripling of this fraction from the inner shells to the outer shells (e.g.,

Aq-B-5). The change in the curvature of the cumulative stellar mass fractions reflects the relative contribution of low- and high-metallicity stars as one moves outwards. In general, in the IHRs, the stellar mass fraction of stars with $[\text{Fe}/\text{H}] > -1$ are between $\sim 40 - 60$ per cent, while in the OHRs they represent less than ~ 20 per cent of the total stellar mass. VMP stars can represent up to ~ 60 per cent of the total stellar mass in the OHRs of the simulated haloes.

Another view of the variation in the predicted MDFs with distance is provided by the mean $[\text{Fe}/\text{H}]$ profiles, shown in the right-hand panels of Fig. 3. The nature of the IHPs determine the slope within the IHRs, but have little effect on the characteristics of the MDF in the OHRs, as we have already seen. Regarding the central regions, where the IHPs dominate, the profiles are strongly affected by the presence of disc-heated and endo-debris stars. In our simulated stellar haloes, the OHPs can contribute up to ~ 40 per cent of the total stellar mass within the IHRs, as can be seen from Fig. 2. Disc-heated and endo-debris stars tend to have lower binding energy, and to be more concentrated in the central regions. As shown in fig. 1 of Paper I, they have a strong influence on the level of enrichment, while both the relative distribution of accreted stars and in situ stars determines the final metallicity profiles within r_{HTR} .

To better quantify the different behaviours seen in the metallicity distribution profiles, we performed linear regressions, of the form $[\text{Fe}/\text{H}] = a * r + b$, from r_{HTR} to 150 kpc, in order to avoid the noise associated with the low number density of stars at the outer limit of the haloes. Excluding the IHRs also makes it easier to estimate a linear regression since, for some haloes, there is a very steep increase of the metallicity in these regions, which precludes an adequate fit with a single linear relation. Two stellar haloes (Aq-C-5 and Aq-G-5) exhibit quite flat slopes in their OHRs (-0.002 dex kpc^{-1}), while the rest have larger slopes, up to ~ -0.01 dex kpc^{-1} (see Table 1). We note that, outside the r_{HTR} , the dominant populations are the OHPs, formed mainly by debris stars (a small fraction of endo-debris stars also contribute in this region).

The masses of the accreted subgalactic systems, together with their gas richness, their baryonic physics (which regulate their star-formation histories), and how the disruption of the satellites occurred within the dark matter haloes, are important mechanisms that shape the MDFs in the OHRs; these are naturally taken into account in our simulations. Indeed, Cooper et al. (2010) and Gómez et al.

(2012) used analytical models grafted onto the dark-matter only simulations of the same haloes (albeit with higher numerical resolution than we explore here), and found very weak or flat slopes. In the case of Cooper et al. (2010), the authors pointed out that those haloes which experienced massive accretions exhibited steeper profiles. This is consistent with our findings, although we obtain larger (negative) gradients in most of our stellar haloes, which can be understood when the different assembly histories are considered, along with a consistent treatment of the microphysics of the baryons.

The manner in which the subgalactic systems are disrupted and distributed into the haloes is important as well, since the more-massive subgalactic systems will be able to survive farther into the main galaxy, at least in general. Although dynamical friction also depends on their orbital parameters, and hence can modulate the effects of their masses, from our analysis it is clear that high-metallicity stars are more gravitationally bound than low-metallicity stars, as was shown in Paper II by consideration of the distribution of binding energy as a function of metallicity. We thus seek to explore in more detail how subgalactic systems of different masses contributed to the formation of each of the simulated stellar haloes, and how to link them to the characteristics of the MDFs as a function of radius.

4 ACCRETED SUBGALACTIC SYSTEMS

The variation of the properties of the diffuse stellar halo MDFs is determined by how the stellar haloes were assembled. Can the diffuse stellar halo MDFs tell us anything about the systems that contributed to their formation? The upper panels of Fig. 4 show the fraction of stellar-debris mass as a function of the total mass of the subgalactic systems from which it formed, for the IHPs and OHPs of the six analysed Aquarius haloes. The lower panels display the same information, but as cumulative stellar mass. The vertical dashed lines represent the threshold mass adopted to classify the subgalactic systems into more-massive and less-massive ones ($M = 10^9 M_{\odot}$).

The contributions of stars from low-mass subgalactic systems are larger for the OHPs than for the IHPs, as can be clearly seen from both the accreted-mass and the cumulative-mass fractions. For the IHPs, four out of the six simulated haloes have less than ~ 20 per cent of their stellar masses formed in low-mass subgalactic systems. The other two, Aq-A-5 and Aq-C-5, have a larger contribution from low-mass systems, so that only ~ 40 per cent of the stellar masses were formed in massive subgalactic units.

In the case of the OHPs, there are also clearly different behaviours from one simulated halo to the next. Three of the OHPs have more than ~ 60 per cent of their stellar masses formed in low- and intermediate-mass subgalactic systems (Aq-A-5, Aq-C-5 and Aq-G-5), while the other three (Aq-B-5, Aq-D-5 and Aq-H-5) have more than ~ 70 per cent formed from more-massive systems. Paper II showed that there was a correlation between the slope of the metallicity profiles of the OHPs and the fraction of stars formed in massive systems, due to the fact that they are found to have larger fractions of more-bound, higher-metallicity stars. We confirm this finding here, since Aq-B-5, Aq-D-5 and Aq-H-5

are the haloes exhibiting the steeper metallicity slopes, as can be seen from Fig. 3 and Table 1.

The relative contribution of low-mass and high-mass subgalactic systems to the IHPs and OHPs can be better illustrated from Fig. 5 (second and fourth columns, respectively). From this figure, we can see that the stellar haloes with the steeper [Fe/H] profiles have more important contributions from stars formed in massive satellites at all radii. As one moves to haloes with flatter metallicity profiles, the relative contribution of low-mass satellites increases, so that the stellar halo with the flatter slope is dominated by the contribution of stars formed in low-mass satellites at all radii. In the case of Aq-G-5, we can clearly see the difference in the debris assembly between the IHP and OHP, which is responsible for the sharp change in the MDF.

Massive subgalactic systems are expected to contribute a significant fraction of high-metallicity stars to both the IHPs and OHPs. They will also survive farther into the haloes, contributing to setting the nature of the metallicity profiles. In order to clearly show how subgalactic systems contribute stars of different metallicities, Fig. 5 shows the cumulative mass fraction as a function of [Fe/H], for debris stars formed in more-massive and less-massive accreted satellites, for both the IHPs and OHPs of our simulated haloes (first and third columns, respectively). They have been ordered, from upper left to lower right, according to the slope of the total [Fe/H] profiles, from the steepest to the flattest ones. Regarding the IHPs, more than ~ 80 per cent of the debris stars come from satellites more massive than $10^9 M_{\odot}$, which also contribute most of the high-metallicity stars. Aq-A-5 and Aq-C-5 are the only simulations that exhibit significant contributions from lower-mass subgalactic systems for the IHPs (recall that the IHPs also received important contributions from in situ stars, which can modify their metallicity profiles).

From Fig. 5 it is clear that, while massive subgalactic systems contribute most of the high-metallicity stars, the low-metallicity stars can come from low-mass, intermediate-mass and massive systems. However, stellar haloes with the flatter slopes tend to have important contributions from low-mass subgalactic systems. This figure allows us to understand the shape of the cumulative stellar mass shown in Fig. 3 for Aq-C-5 and A-G-5. The convex shape of the latter is produced by more significant contributions from low-metallicity stars formed in lower-mass subgalactic systems, as compared to Aq-C-5.

The fact that the MDF of the diffuse stellar halo for a given galaxy does not change strongly as one moves from the IHR to the OHR does not refute its hierarchical assembly, but rather, suggests that the assembly history of such a galaxy might involve similar contributions from satellites of different masses, which are better mixed within the potential well of the main system, with a clear trend to have the flattest slope in those systems with larger contribution from low-mass satellites.

4.1 Confrontation with observations

Numerous observational efforts are beginning to provide information, not only on the existence of extended, diffuse stellar haloes in the MW and other nearby galaxies, but on their chemical and dynamical properties as well. It is

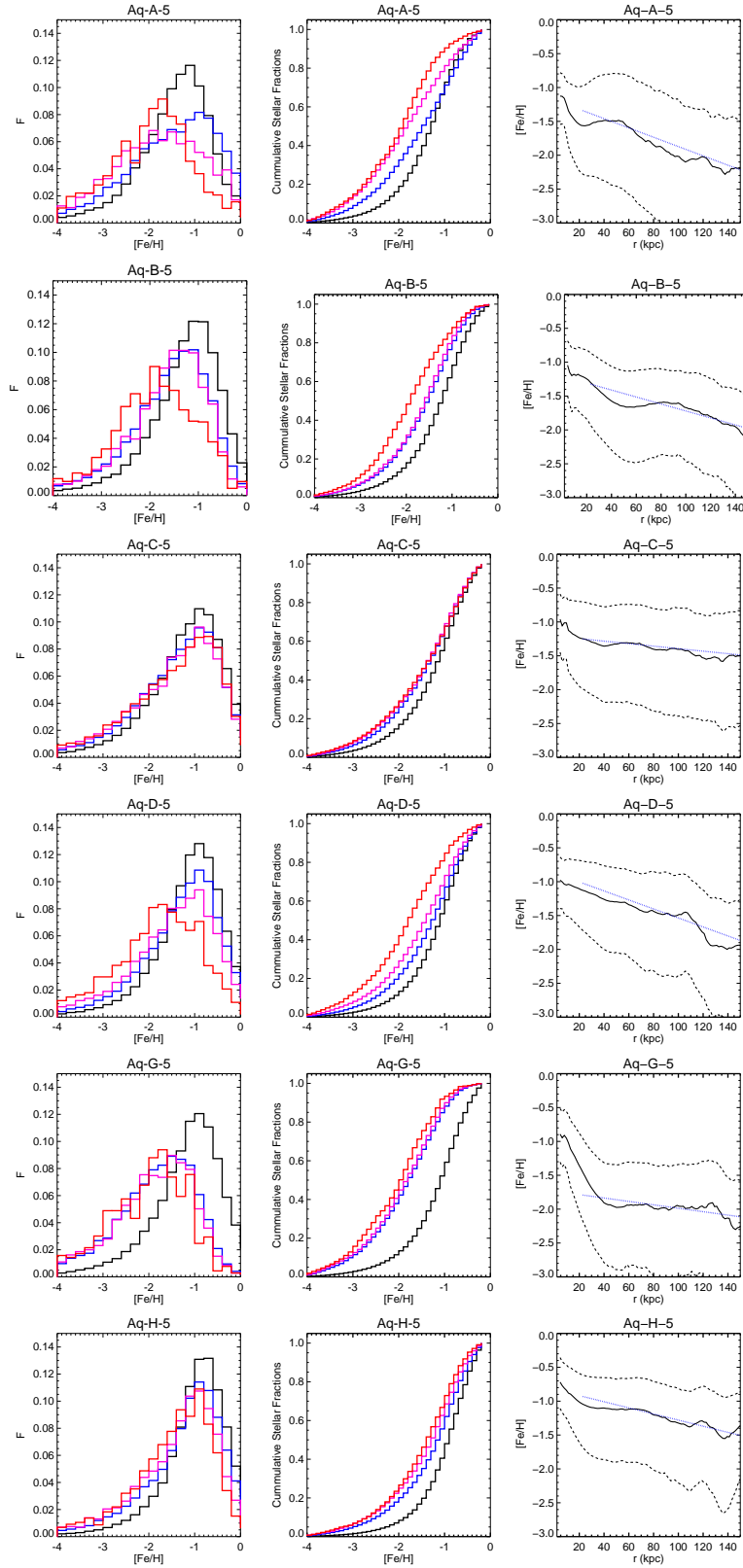


Figure 3. The predicted stellar MDFs (left-hand panels), the cumulative stellar mass (middle panels), and the median metallicity profiles (right-hand panels), as a function of galactocentric distance, for the entire stellar haloes (i.e., combined IHPs and OHPs), estimated in four concentric radial bins at: < 20 kpc (black lines), $20 - 40$ kpc (blue lines), $60 - 80$ kpc (magenta lines) and $80 - 120$ kpc (red lines). The blue line in the right-hand panels show the best fit to the median metallicity profiles for stars in the OHRs of each simulation; the dashed lines represent the second and fourth quartiles.

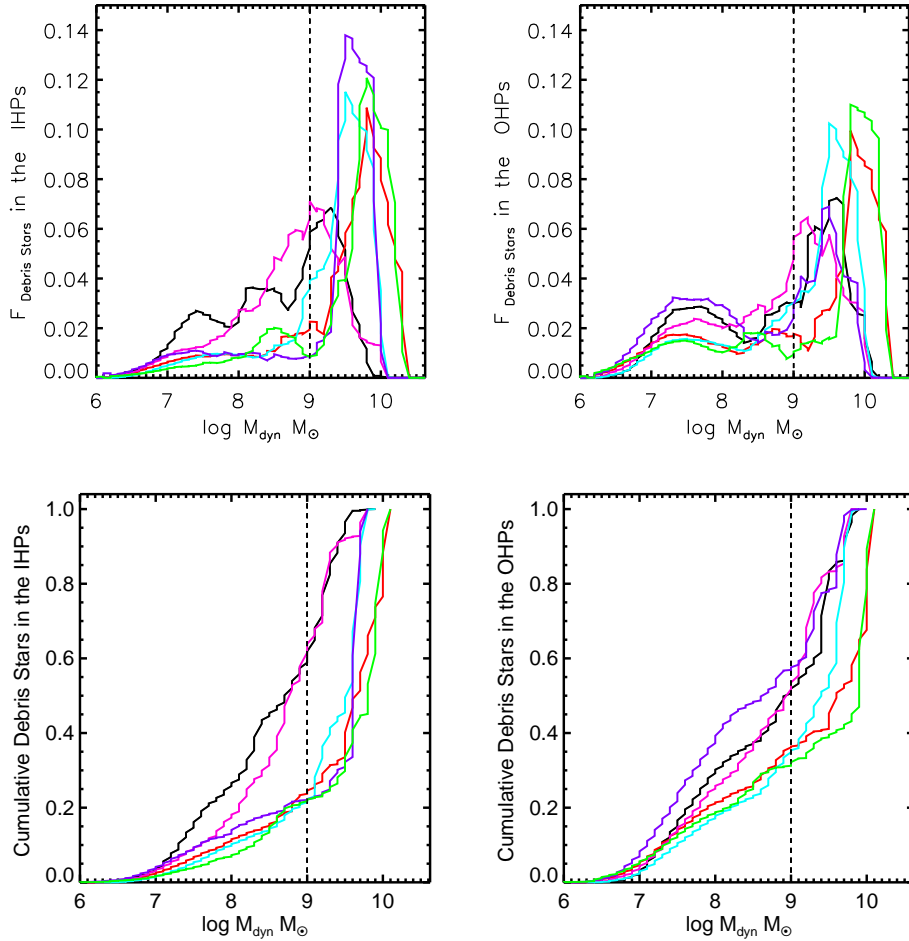


Figure 4. Mass fraction (upper panels) and cumulative mass (lower panels) of debris stars in the IHPs (left panels) and OHPs (right panels), as a function of the dynamical masses of the systems from which they formed. The vertical dashed lines denote the reference value, $M = 10^9 M_{\odot}$, used to separate more-massive from less-massive satellites. See Table 1 for the colour code.

still premature to carry out a detailed statistical comparison between these observations and the simulations, since both lack sufficient numbers of objects (or realizations) to fully represent the range of phenomena that exist. However, even with the limited information available at present, we can compare with the observed variation of the MDFs of the detected stellar haloes in spiral galaxies as one moves from the IHRs to the OHRs, in order to see if our simulated haloes are indeed providing useful insight.

For the purpose of this exercise, we adopt a simple difference between the medians of the $[\text{Fe}/\text{H}]$ distributions for the IHPs and OHPs, $\Delta[\text{Fe}/\text{H}]$. In the case of the observations, $\Delta[\text{Fe}/\text{H}]$ is estimated using the peak values of the MDFs reported by observers to be associated with the likely IHPs and OHPs of the galaxy under consideration, or else is inferred from the CMD-based metallicity profiles. The simulated haloes exhibit a mean $\Delta[\text{Fe}/\text{H}] \sim -0.5$ dex (see also Paper I), well within the range in this parameter covered by current observations (see Fig. 6).

We have also estimated $\Delta[\text{Fe}/\text{H}]$ from the simulations by only considering the portion of the stellar IHPs and OHPs that was contributed by the debris stars. This produced a decrease in the metallicity differences, with a mean

$\Delta[\text{Fe}/\text{H}] \sim -0.35$ (Fig. 6, violet points). The inclusion of the in situ subpopulations generally increases the value of $\Delta[\text{Fe}/\text{H}]$, since the latter contribute more chemically-enriched stars (in particular to the IHPs), although there are outliers. The simulated halo Aq-G-5, for example, exhibits a very large metallicity difference even in the case when only debris stars are considered, and is only weakly affected by addition of the in situ component. Such behaviour results from the particular assembly history of this halo, which produced a very steep MDF profile in the IHP as a result of the contribution from massive satellites, as can be seen in Fig. 5. The other interesting system is Aq-B-5, which has an IHP and OHP dominated by debris stars, but only negligible contributions from the disc-heated subpopulation.

Fig. 6 also displays the observed values reported for the MW, M31 and M32 (Brown et al. 2007; Carollo et al. 2010; Sarajedini et al. 2012; Gilbert et al. 2013), indicated by the different-coloured horizontal lines. We also include an estimate from the CMD metallicity profiles reported by Monachesi et al. (2013) for M81, which implies a flat metallicity gradient, and consequently we assume a $\Delta[\text{Fe}/\text{H}] \sim 0$. As noted above, the observed ranges are in good agreement with our results. According to our simulations, in order

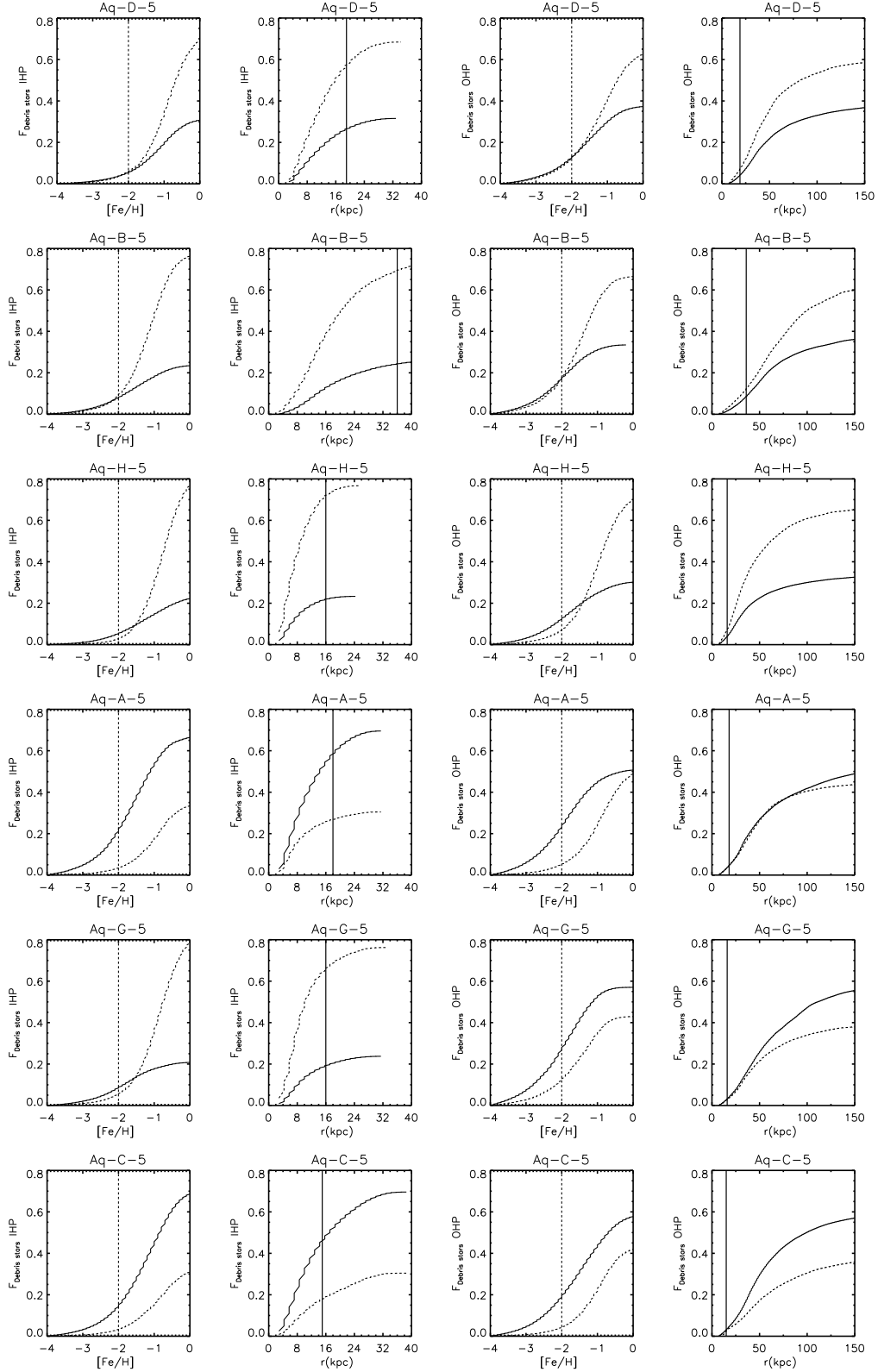


Figure 5. Cumulative stellar mass, as a function of the metallicity of debris stars (first and third columns), and as a function of galactocentric distance (second and fourth columns), formed in less-massive ($M < 10^9 M_{\odot}$, solid lines), and more-massive ($M > 10^9 M_{\odot}$, dashed lines) subgalactic systems, which were accreted to form the IHPs and OHPs of our simulated haloes. The vertical dashed lines denote $[\text{Fe}/\text{H}]$, while the vertical solid lines show the r_{HTR} . The stellar haloes have been ordered from those exhibiting overall steeper to flatter metallicity-profile slopes, from the upper left to the lower right. Flatter overall metallicity slopes can be associated with haloes that have been assembled with a more significant contribution from low-mass satellites. There is a clear transition in the relative contribution of low- and high-mass satellites, which is reflected in the MDF characteristics. There are systems that exhibit quite different behaviours, as expected in hierarchical clustering scenarios.

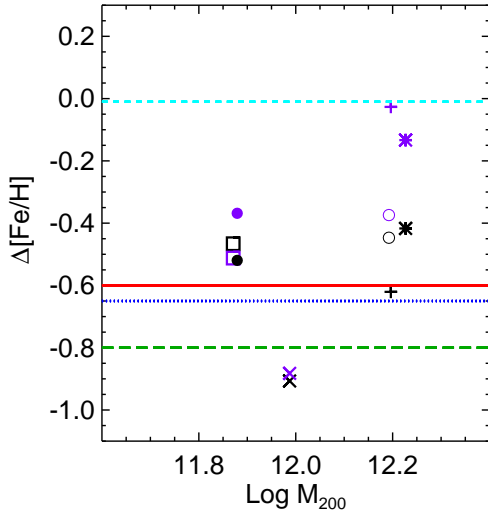


Figure 6. Difference between the median $[\text{Fe}/\text{H}]$ of the IHPs and OHPs, $\Delta[\text{Fe}/\text{H}]$, as a function virial mass, using the entire stellar populations (black symbols) and the debris subpopulations only (violet symbols). The horizontal lines denote the observed values for the MW (Carollo et al. 2010, red solid line), M32 (Sarajedini et al. 2012, blue dotted line) and M31 (Gilbert et al. 2013; Ibata et al. 2014, green dashed lines). We also include a CMD-deduced value for the $[\text{Fe}/\text{H}]$ profile for M81 (Monachesi et al. 2013, cyan dashed line).

to obtain the metallicity difference between the IHPs and OHPs observed for the MW, M32 or M31, a contribution of in situ stars would be required, which suggests the accretion of massive satellites or/and the presence of disc-heated stars. Conversely, for M81, our simulations suggest an assembly history that is dominated by debris stars formed in a satellites of various masses that contributed similar fractions to the stellar halo, with almost no contribution from in situ stars. However, we note that this comparison is fairly rough, as it does not provide clear information on the metallicity profiles.

5 VERY METAL-POOR STARS

The VMP stars, defined as those with $[\text{Fe}/\text{H}] < -2$, can provide information about the nature of the interstellar medium from which they were born, at early stages of the star-formation process. Hence, they have been claimed to provide local windows on the formation of the first subgalactic systems. The commonly adopted hypothesis is that the lower-metallicity stars would come primarily from debris stars, while the higher-metallicity stars would have a larger probability to have been formed in situ. In general terms, VMP stars might better trace the formation of the OHPs. Our simulations agree with these assumptions, at least in the OHRs, but within the IHRs, a more careful analysis is needed.

First, we calculated the frequency of VMP stars in our simulated haloes as a function of galactocentric distance. As shown in Fig. 7, VMP stars represent less than ~ 20 per cent of the total stellar mass within the IHRs, while their percentage increases rapidly in the OHRs. For compar-

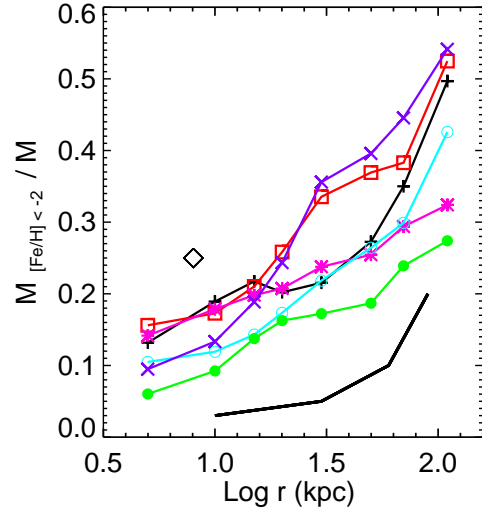


Figure 7. Fraction of the total stellar mass associated with stars with $[\text{Fe}/\text{H}] < -2$, the VMP stars (solid lines, see colour and symbol coding from Table 1). For comparison we include observational estimates for the MW (An et al. 2013, large diamond) and M31 (Gilbert et al. 2013, black thick line).

ison, we include the observed estimates for the Milky Way reported by An et al. (2013), based on an analysis of the photometric MDF of main-sequence stars in SDSS Stripe 82 located between 5 and 8 kpc from the Sun³, and for M31 by Gilbert et al. (2013). The M31 metallicities are photometric estimates for stars that are known members of the M31 giant branch, based on spectroscopic observations. The line shown for this sample represents the fraction of stars bluer than a 10 Gyr, $[\text{Fe}/\text{H}] = -2.0$, solar $[\alpha/\text{Fe}]$ isochrone (VandenBerg et al. 2006). Our simulated values are within the limits established by these two galaxies. In the case of M31, we can appreciate a similar increase of the VMP stars as a function of radius, as expected from our simulations, although it is clear that the halo system of M31 is generally more metal-rich than our simulations. In our stellar haloes, VMP stars are primarily associated with debris subpopulations. The in situ stars represent a small fraction of the VMP stars, with only a very weak dependence on radius. Between ~ 50 per cent and ~ 90 per cent of the VMP debris stars are found to be born in subgalactic systems with $M < 10^9 M_{\odot}$.

Within the IHRs, which includes the fiducial solar neighbourhood, the fraction of VMP stars coming from in situ subpopulations is significant, although it is always less than ~ 40 per cent. Hence, a selection of VMP stars within r_{HTR} would provide, in general, information on the properties of debris stars, but it also could be (in some cases more

³ Note that we have plotted the fraction that An et al. (2013), associate with the low-metallicity (OHP) component in their analysis, ~ 25 per cent, although they indicate that the relative contribution of the OHP component increases with declining metallicity. For $[\text{Fe}/\text{H}] < -2$, this fraction may rise to as high as ~ 50 per cent.

than others) confounded by the presence of in situ subpopulation stars.

The situation changes, however, when additional information, such as that provided by the α -elements, is considered. Within the IHRs, between ~ 55 per cent and ~ 90 per cent of VMP stars with $[\text{O}/\text{Fe}] > 0$ come from accreted subgalactic systems. As expected, these fractions increase for larger radii. Again, the rate of increase depends on the assembly history of each simulated halo. We estimate that the fraction of VMP debris stars originating in low-mass subgalactic systems ranges between $\sim 60 - 90$ per cent. An interesting point is that the contribution from lower-mass subgalactic systems is quite uniform as a function of radius. This is in agreement with the results reported in Paper II, where it was shown that VMP stars cover the entire range of binding energies, while higher-metallicity stars were concentrated towards lower binding energies.

In these simulated haloes, within a fiducial solar neighbourhood, debris stars represent ~ 50 per cent of the total stellar mass of VMP stars. This fraction increases to $\sim 60 - 90$ per cent if the condition of $[\text{O}/\text{Fe}] > 0$ is imposed. More than ~ 70 per cent of VMP stars were formed in subgalactic systems with $M < 10^9 M_\odot$. These fractions should be taken as indicative, not definitive, since they would likely change from halo to halo, and also with the adopted chemical-evolution model. There are results which suggest that metal diffusion might affect the frequency of very low-metallicity stars (e.g. Pilkington et al. 2012), but, in this case, since it affects all simulated systems equally, the trends reported in this work are not expected to change. Moreover, the treatment of metal diffusion should maintain such a trend, since it seems to be already in agreement with observations.

6 CONCLUSIONS

This paper focusses on the study of how the MDF changes in the stellar haloes from the IHRs to the OHRs, and how the characteristics of these changes can be linked to the assembly history of the haloes in hierarchical formation scenarios. Observations have now begun to yield important information on the dynamics and chemical properties of the stellar populations in the MW and nearby galaxies, which can be understood within the current cosmological context.

Our six simulated stellar haloes have total masses between $\sim 10^{10} - 3 \times 10^{10} M_\odot$, values which agree with recent estimates of the total stellar halo of M31 by Ibata et al. (2014). In addition, the stellar mass function of the surviving satellites are well within the observed values for MW and M31 reported recently by McConnachie (2012) and Watkins et al. (2013). The mean metallicity of the stellar haloes correlate with the fraction of stars accreted from massive systems, as discussed in Paper I.

From our study of six MW-mass galaxies simulated within a Λ CDM cosmology, we report the following results:

- The halo transition radius for a given halo, r_{HTR} , defined as the distance where the relative dominance of the diffuse stellar population changes from the IHP to the OHP, is typically $\sim 15 - 20$ kpc (except for one halo which has $r_{\text{HTR}} \sim 36$ kpc). This characteristic radius defines an inner-halo region (IHR) and an outer-halo region (OHR); the IHR

is dominated by the IHP, and the OHR is dominated by the OHP. There is a $\sim 20 - 40$ per cent contribution of the OHPs to the IHRs in our simulations, while the IHP number densities decrease very quickly, and have an almost negligible presence in the OHRs.

- The MDF and the cumulative stellar mass of the total diffuse stellar haloes vary as a function of galactocentric radius. The level of change is different for each simulated system, reflecting their different formation histories. Within the IHR, the in situ component can play a more important role, increasing the mean metallicity. From r_{HTR} out to the virial radius, the stellar haloes are formed primarily by the accretion of satellites with different masses. Nevertheless, some stellar haloes show very small changes from the IHR to the OHR, while others exhibit large metallicity differences.

- The metallicity profiles exhibit behaviours that are consistent with the changes in the MDFs. Our results indicate that mild metallicity gradients are present in the OHRs of those stellar haloes which received important contributions from debris stars formed in massive satellites ($M > 10^9 M_\odot$). Flat gradients in the OHRs are found in those stellar haloes assembled by similar contributions from more-massive and less-massive accreted satellites; the relative contribution of lower-mass subgalactic system is larger in this case than for those with mild gradients.

- Indeed, we found that debris from lower-mass subgalactic systems tends to contribute some $\sim 60 - 90$ per cent of the VMP ($[\text{Fe}/\text{H}] < -2$) stars. These VMP stars cover the entire range of binding energy, hence they are equally distributed within the virial radius. Higher-metallicity stars tend to have lower binding energies, and hence, on average, are more centrally concentrated. VMP stars arise primarily from the debris subpopulations, and the frequency of VMP stars is an increasing function of galactocentric distance. VMP stars belonging to the in situ subpopulation exhibit no trend with radius in our simulations, and account for less than 10 per cent of the total numbers. The increase in the fraction of VMP stars with radius appears to be a characteristic signature of the hierarchical assembly of the haloes via subgalactic accretion.

The analysis presented in this work shows clearly how the contributions from subgalactic systems of different masses form stellar haloes with a range of characteristics, and fix the nature of the chemical properties at different galactocentric distances. Our results show how hierarchical clustering scenarios can naturally reproduce both the presence and the absence of metallicity gradients in the diffuse stellar haloes of large spirals such as the Milky Way. Even so, that there are different numerical caveats related to the sub-grid physics modeling and numerical resolution which need to be improved in future revisions of simulations such as we have explored here. For this purpose, confrontation of the detailed model predictions with the observed chemodynamical properties of galaxies remains a powerful and illuminating tool.

ACKNOWLEDGEMENTS

We thank the referee for his/her comments, which helped to improve the paper. PBT acknowledges the L'Oreal-Unesco

Conicet Award for Women in Science, PICT Raices (2011) of the Ministry of Science and Technology (Argentina), and the Cosmocomp and Lacedal Networks of FP7 Programme of the European Community. TCB acknowledges partial funding from grant PHY 08-22648: Physics Frontier Center / Joint Institute for Nuclear Astrophysics (JINA), awarded by the U.S. National Science Foundation.

REFERENCES

- Abadi M. G., Navarro J. F., Steinmetz M., Eke V. R., 2003, *ApJ*, 591, 499
- Agertz O., Teyssier R., Moore B., 2009, *MNRAS*, 397, L64
- An D., Beers T. C., Johnson J. A., Pinsonneault M. H., Lee Y. S., Bovy J., Ivezić Ž., Carollo D., Newby M., 2013, *ApJ*, 763, 65
- Aumer M., White S. D. M., Naab T., Scannapieco C., 2013, *MNRAS*, 434, 3142
- Beers T. C., Carollo D., Ivezić Ž., An D., Chiba M., Norris J. E., Freeman K. C., Lee Y. S., Munn J. A., Re Fiorentin P., Sivarani T., Wilhelm R., Yanny B., York D. G., 2012, *ApJ*, 746, 34
- Brown T. M., Smith E., Ferguson H. C., Guhathakurta P., Kalirai J. S., Rich R. M., Renzini A., Sweigart A. V., Reitzel D., Gilbert K. M., Geha M., 2007, *ApJL*, 658, L95
- Bullock J. S., Johnston K. V., 2005, *ApJ*, 635, 931
- Carollo D., Beers T. C., Chiba M., Norris J. E., Freeman K. C., Lee Y. S., Ivezić Ž., Rockosi C. M., Yanny B., 2010, *ApJ*, 712, 692
- Carollo D., Beers T. C., Lee Y. S., Chiba M., Norris J. E., Wilhelm R., Sivarani T., Marsteller B., Munn J. A., Bailer-Jones C. A. L., Fiorentin P. R., York D. G., 2007, *Nature*, 450, 1020
- Cooper A. P., Cole S., Frenk C. S., White S. D. M., Helly J., Benson A. J., De Lucia G., Helmi A., Jenkins A., Navarro J. F., Springel V., Wang J., 2010, *MNRAS*, 406, 744
- de Jong J. T. A., Yanny B., Rix H.-W., Dolphin A. E., Martin N. F., Beers T. C., 2010, *ApJ*, 714, 663
- De Rossi M. E., Avila-Reese V., Tissera P. B., González-Samaniego A., Pedrosa S. E., 2013, *MNRAS*, 435, 2736
- Dorman C. E., Widrow L. M., Guhathakurta P., Seth A. C., Foreman-Mackey D., Bell E. F., Dalcanton J. J., Gilbert K. M., Skillman E. D., Williams B. F., 2013, *ApJ*, 779, 103
- Font A. S., McCarthy I. G., Crain R. A., Theuns T., Schaye J., Wiersma R. P. C., Dalla Vecchia C., 2011, *MNRAS*, 416, 2802
- Gilbert K., Beaton R., Bullock J., Chiba M., Geha M. C., Guhathakurta P., Kalirai J. S., Kirby E. N., Majewski S. R., Patterson R. J., Tanaka M., Tollerud E. J., SPLASH Collaboration 2013, in *American Astronomical Society Meeting Abstracts Vol. 221 of American Astronomical Society Meeting Abstracts, The SPLASH Survey: Surface Brightness Profile and Metallicity Gradient of Andromeda's Stellar Halo*. p. 146.16
- Gómez F. A., Coleman-Smith C. E., O'Shea B. W., Tumlinson J., Wolpert R. L., 2012, *ApJ*, 760, 112
- Gómez F. A., Helmi A., Cooper A. P., Frenk C. S., Navarro J. F., White S. D. M., 2013, *MNRAS*, 436, 3602
- Governato F., Brook C. B., Brooks A. M., Mayer L., Willman B., Jonsson P., Stilp A. M., Pope L., Christensen C., Wadsley J., Quinn T., 2009, *MNRAS*, 398, 312
- Guedes J., Callegari S., Madau P., Mayer L., 2011, *ApJ*, 742, 76
- Hopkins P. F., Keres D., Onorbe J., Faucher-Giguere C.-A., Quataert E., Murray N., Bullock J. S., 2013, *ArXiv:1311.2073*
- Ibata R. A., Lewis G. F., McConnachie A. W., Martin N. F., Irwin M. J., Ferguson A. M. N., Babul A., Bernard E. J., Chapman S. C., Collins M., Fardal M., Mackey A. D., Navarro J., Peñarrubia J., Rich R. M., Tanvir N., Widrow L., 2014, *ApJ*, 780, 128
- Ivezić Ž., Beers T. C., Jurić M., 2012, *ARA&A*, 50, 251
- Johnston K. V., Bullock J. S., Sharma S., Font A., Robertson B. E., Leitner S. N., 2008, *ApJ*, 689, 936
- McCarthy I. G., Font A. S., Crain R. A., Deason A. J., Schaye J., Theuns T., 2012, *MNRAS*, 420, 2245
- McConnachie A. W., 2012, *AJ*, 144, 4
- Monachesi A., Bell E. F., Radburn-Smith D. J., Vlajić M., de Jong R. S., Bailin J., Dalcanton J. J., Holwerda B. W., Streich D., 2013, *ApJ*, 766, 106
- Nissen P. E., Schuster W. J., 2010, *A&A*, 511, L10
- Pilkington K., Gibson B. K., Brook C. B., Calura F., Stinson G. S., Thacker R. J., Michel-Dansac L., Bailin J., Couchman H. M. P., Wadsley J., Quinn T. R., Maccio A., 2012, *MNRAS*, 425, 969
- Purcell C. W., Kazantzidis S., Bullock J. S., 2009, *ApJL*, 694, L98
- Sarajedini A., Yang S.-C., Monachesi A., Lauer T. R., Trager S. C., 2012, *MNRAS*, 425, 1459
- Sawala T., Scannapieco C., White S., 2012, *MNRAS*, 420, 1714
- Scannapieco C., Tissera P. B., White S. D. M., Springel V., 2005, *MNRAS*, 364, 552
- Scannapieco C., Tissera P. B., White S. D. M., Springel V., 2006, *MNRAS*, 371, 1125
- Scannapieco C., White S. D. M., Springel V., Tissera P. B., 2009, *MNRAS*, 396, 696
- Scannapieco C., White S. D. M., Springel V., Tissera P. B., 2011, *MNRAS*, 417, 154
- Springel V., Wang J., Vogelsberger M., Ludlow A., Jenkins A., Helmi A., Navarro J. F., Frenk C. S., White S. D. M., 2008, *MNRAS*, 391, 1685
- Stinson G. S., Brook C., Macciò A. V., Wadsley J., Quinn T. R., Couchman H. M. P., 2013, *MNRAS*, 428, 129
- Tissera P. B., Scannapieco C., Beers T. C., Carollo D., 2013, *MNRAS*, 432, 3391
- Tissera P. B., White S. D. M., Scannapieco C., 2012, *MNRAS*, 420, 255
- Trujillo I., Bakos J., 2013, *MNRAS*, 431, 1121
- VandenBerg D. A., Bergbusch P. A., Dowler P. D., 2006, *ApJS*, 162, 375
- Watkins L. L., Evans N. W., van de Ven G., 2013, *MNRAS*, 430, 971
- Zolotov A., Willman B., Brooks A. M., Governato F., Brook C. B., Hogg D. W., Quinn T., Stinson G., 2009, *ApJ*, 702, 1058
- Zolotov A., Willman B., Brooks A. M., Governato F., Hogg D. W., Shen S., Wadsley J., 2010, *ApJ*, 721, 738